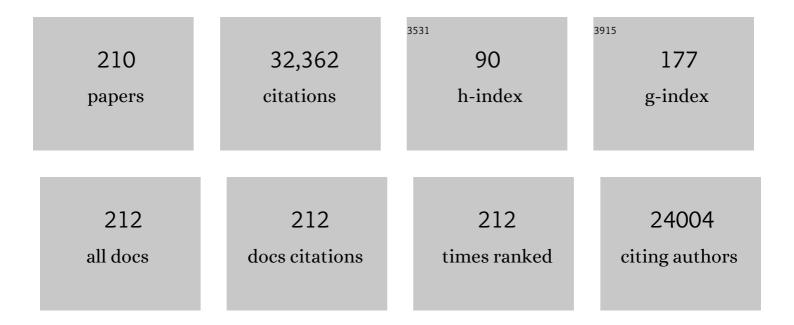
List of Publications by Year in descending order

Source: https://exaly.com/author-pdf/8373260/publications.pdf Version: 2024-02-01



#	Article	IF	CITATIONS
1	Effects of F-Doping on the Photocatalytic Activity and Microstructures of Nanocrystalline TiO2Powders. Chemistry of Materials, 2002, 14, 3808-3816.	6.7	2,068
2	The Effect of Calcination Temperature on the Surface Microstructure and Photocatalytic Activity of TiO2 Thin Films Prepared by Liquid Phase Deposition. Journal of Physical Chemistry B, 2003, 107, 13871-13879.	2.6	1,113
3	In Situ Construction of g-C ₃ N ₄ /g-C ₃ N ₄ Metal-Free Heterojunction for Enhanced Visible-Light Photocatalysis. ACS Applied Materials & Interfaces, 2013, 5, 11392-11401.	8.0	1,102
4	Sulfur-doped g-C3N4 with enhanced photocatalytic CO2-reduction performance. Applied Catalysis B: Environmental, 2015, 176-177, 44-52.	20.2	919
5	Review on the improvement of the photocatalytic and antibacterial activities of ZnO. Journal of Alloys and Compounds, 2017, 727, 792-820.	5.5	884
6	Efficient Visible-Light-Induced Photocatalytic Disinfection on Sulfur-Doped Nanocrystalline Titania. Environmental Science & Technology, 2005, 39, 1175-1179.	10.0	754
7	Isoelectric point and adsorption activity of porous g-C3N4. Applied Surface Science, 2015, 344, 188-195.	6.1	753
8	A Hierarchical Z-Scheme CdS-WO ₃ Photocatalyst with Enhanced CO ₂ Reduction Activity. Small, 2015, 11, 5262-5271.	10.0	682
9	2D/2D/0D TiO2/C3N4/Ti3C2 MXene composite S-scheme photocatalyst with enhanced CO2 reduction activity. Applied Catalysis B: Environmental, 2020, 272, 119006.	20.2	604
10	Fabrication and photocatalytic activity enhanced mechanism of direct Z-scheme g-C 3 N 4 /Ag 2 WO 4 photocatalyst. Applied Surface Science, 2017, 391, 175-183.	6.1	601
11	Preparation and Photocatalytic Behavior of MoS2 and WS2 Nanocluster Sensitized TiO2. Langmuir, 2004, 20, 5865-5869.	3.5	519
12	Effects of acidic and basic hydrolysis catalysts on the photocatalytic activity and microstructures of bimodal mesoporous titania. Journal of Catalysis, 2003, 217, 69-69.	6.2	518
13	A review on TiO2-based Z-scheme photocatalysts. Chinese Journal of Catalysis, 2017, 38, 1936-1955.	14.0	511
14	Selective photocatalytic N ₂ fixation dependent on g-C ₃ N ₄ induced by nitrogen vacancies. Journal of Materials Chemistry A, 2015, 3, 23435-23441.	10.3	495
15	Enhanced photocatalytic H2-production activity of WO3/TiO2 step-scheme heterojunction by graphene modification. Chinese Journal of Catalysis, 2020, 41, 9-20.	14.0	458
16	Noble Metal-Like Behavior of Plasmonic Bi Particles as a Cocatalyst Deposited on (BiO) ₂ CO ₃ Microspheres for Efficient Visible Light Photocatalysis. ACS Catalysis, 2014, 4, 4341-4350.	11.2	441
17	Review on Metal Sulphideâ€based Zâ€scheme Photocatalysts. ChemCatChem, 2019, 11, 1394-1411.	3.7	439
18	Immobilization of Polymeric g-C ₃ N ₄ on Structured Ceramic Foam for Efficient Visible Light Photocatalytic Air Purification with Real Indoor Illumination. Environmental Science & Technology, 2014, 48, 10345-10353.	10.0	436

#	Article	IF	CITATIONS
19	Efficient Photocatalytic Removal of NO in Indoor Air with Hierarchical Bismuth Oxybromide Nanoplate Microspheres under Visible Light. Environmental Science & Technology, 2009, 43, 4143-4150.	10.0	426
20	Review on nanoscale Bi-based photocatalysts. Nanoscale Horizons, 2018, 3, 464-504.	8.0	421
21	Enhanced visible light photocatalytic activity and oxidation ability of porous graphene-like g-C3N4 nanosheets via thermal exfoliation. Applied Surface Science, 2015, 358, 393-403.	6.1	378
22	Graphene-Based Photocatalysts for CO ₂ Reduction to Solar Fuel. Journal of Physical Chemistry Letters, 2015, 6, 4244-4251.	4.6	368
23	Photocatalytic Activity, Antibacterial Effect, and Photoinduced Hydrophilicity of TiO2Films Coated on a Stainless Steel Substrate. Environmental Science & Steinless Steel Substrate. Environmental Science & Steinless Steel Substrate.	10.0	359
24	Synthesis of hierarchical nanoporous F-doped TiO2 spheres with visible light photocatalytic activity. Chemical Communications, 2006, , 1115.	4.1	359
25	Engineering the nanoarchitecture and texture of polymeric carbon nitride semiconductor for enhanced visible light photocatalytic activity. Journal of Colloid and Interface Science, 2013, 401, 70-79.	9.4	358
26	3D hierarchical graphene oxide-NiFe LDH composite with enhanced adsorption affinity to Congo red, methyl orange and Cr(VI) ions. Journal of Hazardous Materials, 2019, 369, 214-225.	12.4	329
27	Water-assisted production of honeycomb-like g-C ₃ N ₄ with ultralong carrier lifetime and outstanding photocatalytic activity. Nanoscale, 2015, 7, 2471-2479.	5.6	328
28	Design, Fabrication, and Mechanism of Nitrogenâ€Doped Grapheneâ€Based Photocatalyst. Advanced Materials, 2021, 33, e2003521.	21.0	324
29	Preparation of highly photocatalytic active nano-sized TiO2 particles via ultrasonic irradiation. Chemical Communications, 2001, , 1942-1943.	4.1	321
30	Workability and mechanical properties of alkali-activated fly ash-slag concrete cured at ambient temperature. Construction and Building Materials, 2018, 172, 476-487.	7.2	305
31	Hybridization of rutile TiO2 (rTiO2) with g-C3N4 quantum dots (CN QDs): An efficient visible-light-driven Z-scheme hybridized photocatalyst. Applied Catalysis B: Environmental, 2017, 202, 611-619.	20.2	296
32	Effect of Carbon Doping on the Mesoporous Structure of Nanocrystalline Titanium Dioxide and Its Solar-Light-Driven Photocatalytic Degradation of NO <i>_x</i> . Langmuir, 2008, 24, 3510-3516.	3.5	288
33	S‣cheme Heterojunction TiO ₂ /CdS Nanocomposite Nanofiber as H ₂ â€Production Photocatalyst. ChemCatChem, 2019, 11, 6301-6309.	3.7	286
34	Photocatalytic H2 evolution on graphdiyne/g-C3N4 hybrid nanocomposites. Applied Catalysis B: Environmental, 2019, 255, 117770.	20.2	284
35	Copolymerization with 2,4,6-Triaminopyrimidine for the Rolling-up the Layer Structure, Tunable Electronic Properties, and Photocatalysis of g-C ₃ N ₄ . ACS Applied Materials & Interfaces, 2015, 7, 5497-5505.	8.0	264
36	Environment-Friendly Carbon Quantum Dots/ZnFe ₂ O ₄ Photocatalysts: Characterization, Biocompatibility, and Mechanisms for NO Removal. Environmental Science & Technology, 2017, 51, 2924-2933.	10.0	260

#	Article	IF	CITATIONS
37	Effects of calcination temperature on the photocatalytic activity and photo-induced super-hydrophilicity of mesoporous TiO2 thin films. New Journal of Chemistry, 2002, 26, 607-613.	2.8	247
38	Low-temperature hydrothermal synthesis of S-doped TiO2 with visible light photocatalytic activity. Journal of Solid State Chemistry, 2006, 179, 1171-1176.	2.9	245
39	DRIFT Study of the SO ₂ Effect on Low-Temperature SCR Reaction over Feâ^'Mn/TiO ₂ . Journal of Physical Chemistry C, 2010, 114, 4961-4965.	3.1	232
40	Novel in Situ N-Doped (BiO) ₂ CO ₃ Hierarchical Microspheres Self-Assembled by Nanosheets as Efficient and Durable Visible Light Driven Photocatalyst. Langmuir, 2012, 28, 766-773.	3.5	218
41	Interfacial Hydrothermal Synthesis of Cu@Cu ₂ O Coreâ^'Shell Microspheres with Enhanced Visible-Light-Driven Photocatalytic Activity. Journal of Physical Chemistry C, 2009, 113, 20896-20902.	3.1	217
42	Fabrication of Bi2O2CO3/g-C3N4 heterojunctions for efficiently photocatalytic NO in air removal: In-situ self-sacrificial synthesis, characterizations and mechanistic study. Applied Catalysis B: Environmental, 2016, 199, 123-133.	20.2	214
43	Roles of N-Vacancies over Porous g-C ₃ N ₄ Microtubes during Photocatalytic NO <i>_x</i> Removal. ACS Applied Materials & Interfaces, 2019, 11, 10651-10662.	8.0	210
44	Efficient Visible Light Photocatalytic Removal of NO with BiOBr-Graphene Nanocomposites. Journal of Physical Chemistry C, 2011, 115, 25330-25337.	3.1	208
45	Hierarchical porous Ni/Co-LDH hollow dodecahedron with excellent adsorption property for Congo red and Cr(VI) ions. Applied Surface Science, 2019, 478, 981-990.	6.1	204
46	Ultrasonic Spray Pyrolysis Synthesis of Porous Bi ₂ WO ₆ Microspheres and Their Visible-Light-Induced Photocatalytic Removal of NO. Journal of Physical Chemistry C, 2010, 114, 6342-6349.	3.1	195
47	Carbon vacancy-induced enhancement of the visible light-driven photocatalytic oxidation of NO over g-C 3 N 4 nanosheets. Applied Surface Science, 2018, 430, 380-389.	6.1	189
48	Hierarchically CdS–Ag2S nanocomposites for efficient photocatalytic H2 production. Applied Surface Science, 2019, 470, 196-204.	6.1	189
49	Enhancement in the photocatalytic H2 production activity of CdS NRs by Ag2S and NiS dual cocatalysts. Applied Catalysis B: Environmental, 2021, 288, 119994.	20.2	189
50	Metal-free disinfection effects induced by graphitic carbon nitride polymers under visible light illumination. Chemical Communications, 2014, 50, 4338.	4.1	187
51	Enhancing effects of water content and ultrasonic irradiation on the photocatalytic activity of nano-sized TiO2 powders. Journal of Photochemistry and Photobiology A: Chemistry, 2002, 148, 263-271.	3.9	173
52	CdIn2S4 microsphere as an efficient visible-light-driven photocatalyst for bacterial inactivation: Synthesis, characterizations and photocatalytic inactivation mechanisms. Applied Catalysis B: Environmental, 2013, 129, 482-490.	20.2	170
53	Biomolecule-controlled hydrothermal synthesis of C–N–S-tridoped TiO2 nanocrystalline photocatalysts for NO removal under simulated solar light irradiation. Journal of Hazardous Materials, 2009, 169, 77-87.	12.4	168
54	Synthesis of a Bi2O2CO3/ZnFe2O4 heterojunction with enhanced photocatalytic activity for visible light irradiation-induced NO removal. Applied Catalysis B: Environmental, 2018, 234, 70-78.	20.2	167

#	Article	IF	CITATIONS
55	High-surface area mesoporous Pt/TiO 2 hollow chains for efficient formaldehyde decomposition at ambient temperature. Journal of Hazardous Materials, 2016, 301, 522-530.	12.4	162
56	Effects of Trifluoroacetic Acid Modification on the Surface Microstructures and Photocatalytic Activity of Mesoporous TiO2Thin Films. Langmuir, 2003, 19, 3889-3896.	3.5	160
57	Facile synthesis of porous graphene-like carbon nitride (C6N9H3) with excellent photocatalytic activity for NO removal. Applied Catalysis B: Environmental, 2015, 174-175, 477-485.	20.2	159
58	A Simple and General Method for the Synthesis of Multicomponent Na2V6O16·3H2O Single-Crystal Nanobelts. Journal of the American Chemical Society, 2004, 126, 3422-3423.	13.7	158
59	Self doping promoted photocatalytic removal of no under visible light with bi2moo6: Indispensable role of superoxide ions. Applied Catalysis B: Environmental, 2016, 182, 316-325.	20.2	157
60	Veterinary antibiotics in food, drinking water, and the urine of preschool children in Hong Kong. Environment International, 2017, 108, 246-252.	10.0	155
61	Preparation, characterization and photocatalytic activity of in situ Fe-doped TiO2 thin films. Thin Solid Films, 2006, 496, 273-280.	1.8	154
62	Self-assembly synthesis of boron-doped graphitic carbon nitride hollow tubes for enhanced photocatalytic NOx removal under visible light. Applied Catalysis B: Environmental, 2018, 239, 352-361.	20.2	154
63	Photocatalytic activity of Ag ₂ MO ₄ (M = Cr, Mo, W) photocatalysts. Journal of Materials Chemistry A, 2015, 3, 20153-20166.	10.3	152
64	Improving photoanodes to obtain highly efficient dye-sensitized solar cells: a brief review. Materials Horizons, 2017, 4, 319-344.	12.2	152
65	Rose-like monodisperse bismuth subcarbonate hierarchical hollow microspheres: One-pot template-free fabrication and excellent visible light photocatalytic activity and photochemical stability for NO removal in indoor air. Journal of Hazardous Materials, 2011, 195, 346-354.	12.4	151
66	Review on nickel-based adsorption materials for Congo red. Journal of Hazardous Materials, 2021, 403, 123559.	12.4	148
67	Sonochemical synthesis and visible light photocatalytic behavior of CdSe and CdSe/TiO2 nanoparticles. Journal of Molecular Catalysis A, 2006, 247, 268-274.	4.8	146
68	Vehicular emission of volatile organic compounds (VOCs) from a tunnel study in Hong Kong. Atmospheric Chemistry and Physics, 2009, 9, 7491-7504.	4.9	143
69	Template-free fabrication and growth mechanism of uniform (BiO)2CO3 hierarchical hollow microspheres with outstanding photocatalytic activities under both UV and visible light irradiation. Journal of Materials Chemistry, 2011, 21, 12428.	6.7	142
70	Growth of BiOBr nanosheets on C3N4 nanosheets to construct two-dimensional nanojunctions with enhanced photoreactivity for NO removal. Journal of Colloid and Interface Science, 2014, 418, 317-323.	9.4	136
71	Hierarchical NiO–SiO2 composite hollow microspheres with enhanced adsorption affinity towards Congo red in water. Journal of Colloid and Interface Science, 2016, 466, 238-246.	9.4	133
72	Visible-Light-Active Plasmonic Ag–SrTiO ₃ Nanocomposites for the Degradation of NO in Air with High Selectivity. ACS Applied Materials & Interfaces, 2016, 8, 4165-4174.	8.0	132

#	Article	IF	CITATIONS
73	Light-induced super-hydrophilicity and photocatalytic activity of mesoporous TiO2 thin films. Journal of Photochemistry and Photobiology A: Chemistry, 2002, 148, 331-339.	3.9	131
74	Enhanced visible-light-driven photocatalytic removal of NO: Effect on layer distortion on g-C3N4 by H2 heating. Applied Catalysis B: Environmental, 2015, 179, 106-112.	20.2	131
75	Perovskite LaFeO3-SrTiO3 composite for synergistically enhanced NO removal under visible light excitation. Applied Catalysis B: Environmental, 2017, 204, 346-357.	20.2	127
76	g ₃ N ₄ â€Based 2D/2D Composite Heterojunction Photocatalyst. Small Structures, 2021, 2, 2100086.	12.0	127
77	Biocompatible FeOOH-Carbon quantum dots nanocomposites for gaseous NO removal under visible light: Improved charge separation and High selectivity. Journal of Hazardous Materials, 2018, 354, 54-62.	12.4	126
78	Halogen poisoning effect of Pt-TiO2 for formaldehyde catalytic oxidation performance at room temperature. Applied Surface Science, 2016, 364, 808-814.	6.1	124
79	Protonated g-C3N4/Ti3+ self-doped TiO2 nanocomposite films: Room-temperature preparation, hydrophilicity, and application for photocatalytic NO removal. Applied Catalysis B: Environmental, 2019, 240, 122-131.	20.2	122
80	Synthesis and adsorption performance of Mg(OH)2 hexagonal nanosheet–graphene oxide composites. Applied Surface Science, 2015, 332, 121-129.	6.1	121
81	Effects of alcohol content and calcination temperature on the textural properties of bimodally mesoporous titania. Applied Catalysis A: General, 2003, 255, 309-320.	4.3	117
82	Direct Z-scheme porous g-C3N4/BiOI heterojunction for enhanced visible-light photocatalytic activity. Journal of Alloys and Compounds, 2018, 766, 841-850.	5.5	115
83	NiFe-LDH nanosheet/carbon fiber nanocomposite with enhanced anionic dye adsorption performance. Applied Surface Science, 2020, 511, 145570.	6.1	112
84	Aerosol-assisted flow synthesis of B-doped, Ni-doped and B–Ni-codoped TiO2 solid and hollow microspheres for photocatalytic removal of NO. Applied Catalysis B: Environmental, 2009, 89, 398-405.	20.2	102
85	Improving g-C3N4 photocatalysis for NOx removal by Ag nanoparticles decoration. Applied Surface Science, 2015, 358, 356-362.	6.1	101
86	Fabrication and enhanced CO2 reduction performance of N-self-doped TiO2 microsheet photocatalyst by bi-cocatalyst modification. Journal of CO2 Utilization, 2016, 16, 442-449.	6.8	99
87	Improved Oxygen Activation over a Carbon/Co ₃ O ₄ Nanocomposite for Efficient Catalytic Oxidation of Formaldehyde at Room Temperature. Environmental Science & Technology, 2021, 55, 4054-4063.	10.0	97
88	Core–shell Fe–Fe2O3 nanostructures as effective persulfate activator for degradation of methyl orange. Separation and Purification Technology, 2013, 108, 159-165.	7.9	95
89	Photocatalytic selective oxidation of phenol to produce dihydroxybenzenes in a TiO 2 /UV system: Hydroxyl radical versus hole. Applied Catalysis B: Environmental, 2016, 199, 405-411.	20.2	95
90	Enhanced visible-light photo-oxidation of nitric oxide using bismuth-coupled graphitic carbon nitride composite heterostructures. Chinese Journal of Catalysis, 2017, 38, 321-329.	14.0	95

#	Article	IF	CITATIONS
91	Enhancing the photocatalytic activity of bulk g-C3N4 by introducing mesoporous structure and hybridizing with graphene. Journal of Colloid and Interface Science, 2014, 436, 29-36.	9.4	92
92	Photocatalytic NO removal on BiOI surface: The change from nonselective oxidation to selective oxidation to selective oxidation. Applied Catalysis B: Environmental, 2015, 168-169, 490-496.	20.2	88
93	Plasmonic Bi/ZnWO ₄ Microspheres with Improved Photocatalytic Activity on NO Removal under Visible Light. ACS Sustainable Chemistry and Engineering, 2016, 4, 6912-6920.	6.7	88
94	Oxygen vacancy–engineered Β-MnO /activated carbon for room-temperature catalytic oxidation of formaldehyde. Applied Catalysis B: Environmental, 2020, 278, 119294.	20.2	87
95	Enhanced solar-to-chemical energy conversion of graphitic carbon nitride by two-dimensional cocatalysts. EnergyChem, 2021, 3, 100051.	19.1	87
96	Enhanced catalytic activity of hierarchically macro-/mesoporous Pt/TiO ₂ toward room-temperature decomposition of formaldehyde. Catalysis Science and Technology, 2015, 5, 2366-2377.	4.1	86
97	TiO2/In2S3 S-scheme photocatalyst with enhanced H2O2-production activity. Nano Research, 2023, 16, 4506-4514.	10.4	85
98	Nearâ€Infraredâ€Responsive Photocatalysts. Small Methods, 2021, 5, e2001042.	8.6	84
99	Sono- and Photochemical Routes for the Formation of Highly Dispersed Gold Nanoclusters in Mesoporous Titania Films. Advanced Functional Materials, 2004, 14, 1178-1183.	14.9	83
100	(NH4)2CO3 mediated hydrothermal synthesis of N-doped (BiO)2CO3 hollow nanoplates microspheres as high-performance and durable visible light photocatalyst for air cleaning. Chemical Engineering Journal, 2013, 214, 198-207.	12.7	83
101	Fabrication of TiO 2 nanorod assembly grafted rGO (rGO@TiO 2 -NR) hybridized flake-like photocatalyst. Applied Surface Science, 2017, 391, 218-227.	6.1	81
102	Enhanced Photocatalytic Activity and Selectivity for CO ₂ Reduction over a TiO ₂ Nanofibre Mat Using Ag and MgO as Bi ocatalyst. ChemCatChem, 2019, 11, 465-472.	3.7	81
103	Photocatalytic CO ₂ reduction of C/ZnO nanofibers enhanced by an Ni-NiS cocatalyst. Nanoscale, 2020, 12, 7206-7213.	5.6	80
104	One-pot template-free synthesis, growth mechanism and enhanced photocatalytic activity of monodisperse (BiO)2CO3 hierarchical hollow microspheres self-assembled with single-crystalline nanosheets. CrystEngComm, 2012, 14, 3534.	2.6	79
105	Graphene-induced formation of visible-light-responsive SnO2-Zn2SnO4 Z-scheme photocatalyst with surface vacancy for the enhanced photoreactivity towards NO and acetone oxidation. Chemical Engineering Journal, 2018, 336, 200-210.	12.7	79
106	Zn Cd1–S quantum dot with enhanced photocatalytic H2-production performance. Chinese Journal of Catalysis, 2021, 42, 15-24.	14.0	79
107	Hierarchical Pt/NiO Hollow Microspheres with Enhanced Catalytic Performance. ChemNanoMat, 2015, 1, 58-67.	2.8	78
108	Tuning the strength of built-in electric field in 2D/2D g-C3N4/SnS2 and g-C3N4/ZrS2 S-scheme heterojunctions by nonmetal doping. Journal of Materiomics, 2021, 7, 988-997.	5.7	77

#	Article	IF	CITATIONS
109	Photocatalytic removal of NO and HCHO over nanocrystalline Zn2SnO4 microcubes for indoor air purification. Journal of Hazardous Materials, 2010, 179, 141-150.	12.4	75
110	Hierarchically porous NiO–Al ₂ O ₃ nanocomposite with enhanced Congo red adsorption in water. RSC Advances, 2016, 6, 10272-10279.	3.6	72
111	Highly enhanced visible-light photocatalytic NO x purification and conversion pathway on self-structurally modified g-C 3 N 4 nanosheets. Science Bulletin, 2018, 63, 609-620.	9.0	72
112	Mass-Controlled Direct Synthesis of Graphene-like Carbon Nitride Nanosheets with Exceptional High Visible Light Activity. Less is Better. Scientific Reports, 2015, 5, 14643.	3.3	71
113	New insights into how RGO influences the photocatalytic performance of BiOIO3/RGO nanocomposites under visible and UV irradiation. Journal of Colloid and Interface Science, 2015, 447, 16-24.	9.4	71
114	Enhanced photocatalytic H2 production performance of CdS hollow spheres using C and Pt as bi-cocatalysts. Chinese Journal of Catalysis, 2021, 42, 743-752.	14.0	67
115	Controllable Synthesis of Core–Shell Bi@Amorphous Bi ₂ O ₃ Nanospheres with Tunable Optical and Photocatalytic Activity for NO Removal. Industrial & Engineering Chemistry Research, 2017, 56, 10251-10258.	3.7	66
116	Controlled synthesis, growth mechanism and highly efficient solar photocatalysis of nitrogen-doped bismuth subcarbonate hierarchical nanosheets architectures. Dalton Transactions, 2012, 41, 8270.	3.3	65
117	In situ Fabrication of α-Bi2O3/(BiO)2CO3 Nanoplate Heterojunctions with Tunable Optical Property and Photocatalytic Activity. Scientific Reports, 2016, 6, 23435.	3.3	65
118	Room-temperature formaldehyde catalytic decomposition. Environmental Science: Nano, 2020, 7, 3655-3709.	4.3	64
119	Effect of mesoporous g-C3N4 substrate on catalytic oxidation of CO over Co3O4. Applied Surface Science, 2017, 401, 333-340.	6.1	63
120	Facile fabrication of porous Cr-doped SrTiO ₃ nanotubes by electrospinning and their enhanced visible-light-driven photocatalytic properties. Journal of Materials Chemistry A, 2015, 3, 3935-3943.	10.3	62
121	Gaseous and particulate polycyclic aromatic hydrocarbons (PAHs) emissions from commercial restaurants in Hong Kong. Journal of Environmental Monitoring, 2007, 9, 1402.	2.1	61
122	Hierarchical porous Al2O3@ZnO core-shell microfibres with excellent adsorption affinity for Congo red molecule. Applied Surface Science, 2019, 473, 251-260.	6.1	61
123	Constructing Z-scheme SnO ₂ /N-doped carbon quantum dots/ZnSn(OH) ₆ nanohybrids with high redox ability for NO <i>x</i> removal under VIS-NIR light. Journal of Materials Chemistry A, 2019, 7, 15782-15793.	10.3	60
124	C3N4 with engineered three coordinated (N3C) nitrogen vacancy boosts the production of 1O2 for Efficient and stable NO photo-oxidation. Chemical Engineering Journal, 2020, 389, 124421.	12.7	60
125	Highly Selective Photocatalytic CO ₂ Methanation with Water Vapor on Singleâ€Atom Platinumâ€Decorated Defective Carbon Nitride. Angewandte Chemie - International Edition, 2022, 61, .	13.8	60
126	Hierarchical porous ZnWO4 microspheres synthesized by ultrasonic spray pyrolysis: Characterization, mechanistic and photocatalytic NO removal studies. Applied Catalysis A: General, 2016, 515, 170-178.	4.3	59

#	Article	IF	CITATIONS
127	Phosphorus flame retardants and Bisphenol A in indoor dust and PM2.5 in kindergartens and primary schools in Hong Kong. Environmental Pollution, 2018, 235, 365-371.	7.5	59
128	Engineering of reduced graphene oxide on nanosheet–g-C3N4/perylene imide heterojunction for enhanced photocatalytic redox performance. Applied Catalysis B: Environmental, 2019, 250, 42-51.	20.2	58
129	Effects of H2O2 generation over visible light-responsive Bi/Bi2O2â^'CO3 nanosheets on their photocatalytic NO removal performance. Chemical Engineering Journal, 2019, 363, 374-382.	12.7	56
130	Structure-Property relationship in β-keto-enamine-based covalent organic frameworks for highly efficient photocatalytic hydrogen production. Chemical Engineering Journal, 2021, 419, 129984.	12.7	56
131	Recent Development of Plasmonic Resonance-Based Photocatalysis and Photovoltaics for Solar Utilization. Molecules, 2016, 21, 180.	3.8	54
132	<i>In situ</i> g-C ₃ N ₄ self-sacrificial synthesis of a g-C ₃ N ₄ /LaCO ₃ OH heterostructure with strong interfacial charge transfer and separation for photocatalytic NO removal. Journal of Materials Chemistry A, 2018, 6, 972-981.	10.3	54
133	Urea and Melamine Formaldehyde Resin-Derived Tubular g-C ₃ N ₄ with Highly Efficient Photocatalytic Performance. ACS Applied Materials & Interfaces, 2019, 11, 27934-27943.	8.0	54
134	Preparation and photocatalytic behavior of MoS2 and WS2 nanocluster sensitized TiO2. Langmuir, 2004, 20, 5865-9.	3.5	54
135	Enhanced photocatalytic removal of NO over titania/hydroxyapatite (TiO ₂ /HAp) composites with improved adsorption and charge mobility ability. RSC Advances, 2017, 7, 24683-24689.	3.6	52
136	Chemical etching fabrication of uniform mesoporous Bi@Bi2O3 nanospheres with enhanced visible light-induced photocatalytic oxidation performance for NOx. Chemical Engineering Journal, 2021, 406, 126910.	12.7	51
137	Preparation of a highly active nanocrystalline TiO2 photocatalyst from titanium oxo cluster precursor. Journal of Solid State Chemistry, 2004, 177, 2584-2590.	2.9	50
138	Construction of the 1D Covalent Organic Framework/2D g-C ₃ N ₄ Heterojunction with High Apparent Quantum Efficiency at 500 nm. ACS Applied Materials & Interfaces, 2020, 12, 51555-51562.	8.0	50
139	Synthesis of SrFexTi1-xO3-l´ nanocubes with tunable oxygen vacancies for selective and efficient photocatalytic NO oxidation. Applied Catalysis B: Environmental, 2018, 239, 1-9.	20.2	46
140	Graphdiyne: A Brilliant Hole Accumulator for Stable and Efficient Planar Perovskite Solar Cells. Small, 2020, 16, e1907290.	10.0	45
141	Enhanced photocatalytic activity and mechanism of CeO2 hollow spheres for tetracycline degradation. Rare Metals, 2021, 40, 2369-2380.	7.1	44
142	Highly photoreactive TiO2 hollow microspheres with super thermal stability for acetone oxidation. Chinese Journal of Catalysis, 2017, 38, 2085-2093.	14.0	42
143	Lowâ€Temperatureâ€Processed Zr/F Coâ€Doped SnO ₂ Electron Transport Layer for Highâ€Efficiency Planar Perovskite Solar Cells. Solar Rrl, 2020, 4, 2000090.	5.8	42
144	Photocatalytic TiO2/Glass Nanoflake Array Films. Langmuir, 2005, 21, 3486-3492.	3.5	41

#	Article	IF	CITATIONS
145	Photocatalytic activity and photo-induced hydrophilicity of mesoporous TiO2 thin films coated on aluminum substrate. Applied Catalysis B: Environmental, 2007, 73, 135-143.	20.2	40
146	Simultaneous excitation of PdCl2 hybrid mesoporous g-C3N4 molecular/solid-state photocatalysts for enhancing the visible-light-induced oxidative removal of nitrogen oxides. Applied Catalysis B: Environmental, 2016, 184, 174-181.	20.2	39
147	Active Complexes on Engineered Crystal Facets of MnO _x –CeO ₂ and Scale-Up Demonstration on an Air Cleaner for Indoor Formaldehyde Removal. Environmental Science & Technology, 2019, 53, 10906-10916.	10.0	36
148	Grapheneâ€Based Materials in Planar Perovskite Solar Cells. Solar Rrl, 2020, 4, 2000502.	5.8	36
149	Characterization of winter airborne particles at Emperor Qin's Terra-cotta Museum, China. Science of the Total Environment, 2009, 407, 5319-5327.	8.0	35
150	Transformation of amorphous Bi2O3 to crystal Bi2O2CO3 on Bi nanospheres surface for photocatalytic NOx oxidation: Intensified hot-electron transfer and reactive oxygen species generation. Chemical Engineering Journal, 2021, 420, 129814.	12.7	35
151	Hierarchical Co3O4-NiO hollow dodecahedron-supported Pt for room-temperature catalytic formaldehyde decomposition. Chemical Engineering Journal, 2022, 430, 132715.	12.7	35
152	Insight into the Photocatalytic Removal of NO in Air over Nanocrystalline Bi ₂ Sn ₂ O ₇ under Simulated Solar Light. Industrial & Engineering Chemistry Research, 2016, 55, 10609-10617.	3.7	34
153	Synthesis of mesoporous polymeric carbon nitride exhibiting enhanced and durable visible light photocatalytic performance. Science Bulletin, 2014, 59, 688-698.	1.7	33
154	Synthesis and characterization of Bi-BiPO4 nanocomposites as plasmonic photocatalysts for oxidative NO removal. Applied Surface Science, 2020, 513, 145775.	6.1	32
155	Graphdiyne-based photocatalysts for solar fuel production. Green Chemistry, 2022, 24, 5739-5754.	9.0	30
156	Metal–Organic Frameworks for NO <i>_x</i> Adsorption and Their Applications in Separation, Sensing, Catalysis, and Biology. Small, 2022, 18, e2105484.	10.0	29
157	A stable single-crystal Bi3NbO7 nanoplates superstructure for effective visible-light-driven photocatalytic removal of nitric oxide. Applied Surface Science, 2012, 263, 266-272.	6.1	28
158	Hydrothermal fabrication of N-doped (BiO)2CO3: Structural and morphological influence on the visible light photocatalytic activity. Applied Surface Science, 2014, 319, 256-264.	6.1	27
159	Novel N/Carbon Quantum Dot Modified MIL-125(Ti) Composite for Enhanced Visible-Light Photocatalytic Removal of NO. Industrial & Engineering Chemistry Research, 2020, 59, 6470-6478.	3.7	26
160	New carbon nitride close to C6N7 with superior visible light absorption for highly efficient photocatalysis. Science Bulletin, 2021, 66, 1764-1772.	9.0	25
161	Nanomaterials for Environmental Applications. Journal of Nanomaterials, 2014, 2014, 1-4.	2.7	24
162	Controllable synthesis of phosphate-modified BiPO ₄ nanorods with high photocatalytic activity: surface hydroxyl groups concentrations effects. RSC Advances, 2015, 5, 99712-99721.	3.6	24

#	Article	IF	CITATIONS
163	Thiourea-Modified TiO2 Nanorods with Enhanced Photocatalytic Activity. Molecules, 2016, 21, 181.	3.8	24
164	Interfacial optimization of Z-scheme Ag3PO4/MoS2 nanoflower sphere heterojunction toward synergistic enhancement of visible-light-driven photocatalytic oxygen evolution and degradation of organic pollutant. Journal of Alloys and Compounds, 2021, 888, 161583.	5.5	24
165	Photocatalytic Air Purification Using Functional Polymeric Carbon Nitrides. Advanced Science, 2021, 8, e2102376.	11.2	24
166	gâ€C ₃ N ₄ /TiO ₂ Composite Film in the Fabrication of a Photocatalytic Airâ€Purifying Pavements. Solar Rrl, 2020, 4, 2000170.	5.8	23
167	Template-free synthesis of ternary sulfides submicrospheres as visible light photocatalysts by ultrasonic spray pyrolysis. Catalysis Science and Technology, 2012, 2, 1825.	4.1	22
168	The role and synergistic effect of the light irradiation and H2O2 in photocatalytic inactivation of Escherichia coli. Journal of Photochemistry and Photobiology B: Biology, 2015, 149, 164-171.	3.8	22
169	Mechanism of NO Photocatalytic Oxidation on g-C3N4 Was Changed by Pd-QDs Modification. Molecules, 2016, 21, 36.	3.8	22
170	Exploring the photocatalytic conversion mechanism of gaseous formaldehyde degradation on TiO2–-OV surface. Journal of Hazardous Materials, 2022, 424, 127217.	12.4	22
171	In-situ synthesis of ternary heterojunctions via g-C3N4 coupling with noble-metal-free NiS and CdS with efficient visible-light-induced photocatalytic H2 evolution and mechanism insight. International Journal of Hydrogen Energy, 2022, 47, 14063-14076.	7.1	22
172	Unraveling the mechanisms of room-temperature catalytic degradation of indoor formaldehyde and its biocompatibility on colloidal TiO ₂ -supported MnO _x –CeO ₂ . Environmental Science: Nano, 2018, 5, 1130-1139.	4.3	21
173	Distribution of bacteria in inhalable particles and its implications for health risks in kindergarten children in Hong Kong. Atmospheric Environment, 2016, 128, 268-275.	4.1	20
174	Ultra violet filters in the urine of preschool children and drinking water. Environment International, 2019, 133, 105246.	10.0	20
175	Reasonable design of Cu2MoS4 heterophase junction for highly efficient photocatalysis. Journal of Alloys and Compounds, 2020, 826, 154076.	5.5	18
176	Highly Selective Photocatalytic CO ₂ Methanation with Water Vapor on Singleâ€Atom Platinumâ€Đecorated Defective Carbon Nitride. Angewandte Chemie, 2022, 134, .	2.0	18
177	Synthesis of flower-like, pinon-like and faceted nanoplates (BiO)2CO3 micro/nanostructures with morphology-dependent photocatalytic activity. Materials Chemistry and Physics, 2013, 142, 381-386.	4.0	17
178	Polyoxometalates-doped Bi2O3–/Bi photocatalyst for highly efficient visible-light photodegradation of tetrabromobisphenol A and removal of NO. Chinese Journal of Catalysis, 2022, 43, 771-781.	14.0	17
179	Aerosol flow synthesis of N, Si-codoped TiO2 hollow microspheres with enhanced visible-light driven photocatalytic performance. Catalysis Communications, 2012, 29, 189-193.	3.3	16
180	Efficient photocatalytic degradation of NO by ceramic foam air filters coated with mesoporous TiO2 thin films. Chinese Journal of Catalysis, 2015, 36, 2109-2118.	14.0	16

#	Article	IF	CITATIONS
181	A Review of Co3O4-based Catalysts for Formaldehyde Oxidation at Low Temperature: Effect Parameters and Reaction Mechanism. Aerosol Science and Engineering, 2020, 4, 147-168.	1.9	16
182	Interfacial optimization of oxygen-vacancy-induced 1D/2D CeO2 nanotubes/g-C3N4 step-scheme heterojunction with enhanced visible-light photocatalysis and mechanism insight. Journal of Alloys and Compounds, 2022, 923, 166330.	5.5	16
183	Fabrication of Bi-Doped <mml:math xmlns:mml="http://www.w3.org/1998/Math/MathML"><mml:mrow><mml:mi>T</mml:mi><mml:msub><mml:mi with Ultrasonic Spray Pyrolysis and Investigation of Their Visible-Light Photocatalytic Properties. lournal of Nanotechnology, 2012, 2012, 1-7.</mml:mi </mml:msub></mml:mrow></mml:math 	>iQ <td>:mi><mml:mi 15</mml:mi </td>	:mi> <mml:mi 15</mml:mi
184	Organophosphate flame retardants and bisphenol A in children's urine in Hong Kong: has the burden been underestimated?. Ecotoxicology and Environmental Safety, 2019, 183, 109502.	6.0	15
185	The photocatalytic NO-removal activity of g-C ₃ N ₄ significantly enhanced by the synergistic effect of Pd ⁰ nanoparticles and N vacancies. Environmental Science: Nano, 2022, 9, 742-750.	4.3	15
186	Construction and Activity of an Allâ€Organic Heterojunction Photocatalyst Based on Melem and Pyromellitic Dianhydride. ChemSusChem, 2022, 15, e202200477.	6.8	15
187	Atmospheric deterioration of Qin brick in an environmental chamber at Emperor Qin's Terracotta Museum, China. Journal of Archaeological Science, 2009, 36, 2578-2583.	2.4	14
188	Peroxymonosulfate activated by amorphous particulate MnO2 for mineralization of benzene gas: Redox reaction, weighting analysis, and numerical modelling. Chemical Engineering Journal, 2017, 316, 61-69.	12.7	14
189	Highly efficient photocatalytic degradation for antibiotics and mechanism insight for Bi2S3/g-C3N4 with fast interfacial charges transfer and excellent stability. Arabian Journal of Chemistry, 2022, 15, 103689.	4.9	12
190	Oxygen vacancy-dependent photocatalytic activity of well-defined Bi ₂ Sn ₂ O _{7â^'x} hollow nanocubes for NO _x removal. Environmental Science: Nano, 2021, 8, 1927-1933.	4.3	11
191	Photocatalytic reactive oxygen species generation activity of TiO ₂ improved by the modification of persistent free radicals. Environmental Science: Nano, 2021, 8, 3846-3854.	4.3	11
192	In Situ Intermediates Determination and Cytotoxicological Assessment in Catalytic Oxidation of Formaldehyde: Implications for Catalyst Design and Selectivity Enhancement under Ambient Conditions. Environmental Science & Technology, 2019, 53, 5230-5240.	10.0	10
193	Facile Synthesis of Visible-Light-Activated F-Doped TiO ₂ Hollow Spheres by Ultrasonic Spray Pyrolysis. Science of Advanced Materials, 2012, 4, 863-868.	0.7	10
194	The photocatalytic •OH production activity of g-C3N4 improved by the introduction of NO. Chinese Chemical Letters, 2022, 33, 4715-4718.	9.0	10
195	Growth-differentiation factor-8 (GDF-8) in the uterus: its identification and functional significance in the golden hamster. Reproductive Biology and Endocrinology, 2009, 7, 134.	3.3	9
196	Efficient Visible Light Photocatalytic Oxidation of NO on F- and N-Codoped Spherical <mml:math xmlns:mml="http://www.w3.org/1998/Math/MathML" id="M1"><mml:mrow><mml:msub><mml:mrow><mml:mtext>TiO</mml:mtext></mml:mrow><mml:mtext mathvariant="bold">2</mml:mtext </mml:msub><mml:msub></mml:msub></mml:mrow>Synthesized via Ultrasonic</mml:math 	2.7	8
197	Spray Pyrolysis. Journal of Nanomaterials, 2012, 2012, 1-9. Nanocasting of Periodic Mesoporous Materials as an Effective Strategy to Prepare Mixed Phases of Titania. Molecules, 2015, 20, 21881-21895.	3.8	8
198	Two-dimensional polyimide heterojunctions for the efficient removal of environmental pollutants under visible-light irradiation. Physical Chemistry Chemical Physics, 2019, 21, 17163-17169.	2.8	8

#	Article	IF	CITATIONS
199	Three-Dimensional Bi \$\$_{5}\$\$ 5 O \$\$_{7}\$\$ 7 I Photocatalysts for Efficient Removal of NO in Air Under Visible Light. Aerosol Science and Engineering, 2017, 1, 33-40.	1.9	6
200	Time-resolved characterization of non-thermal plasma-assisted photocatalytic removal of nitric oxide. Journal Physics D: Applied Physics, 2020, 53, 01LT02.	2.8	4
201	The mechanism of enhanced visible light photocatalysis with micro-structurally optimized and graphene oxide coupled(BiO) ₂ CO ₃ . Chinese Science Bulletin, 2015, 60, 1915-1923.	0.7	3
202	Facile Synthesis of ZnxCd1-xS Solid Solution Microspheres through Ultrasonic Spray Pyrolysis for Improved Photocatalytic Activity. Journal of Nanomaterials, 2017, 2017, 1-8.	2.7	2
203	石墨型C ₃ N ₄ 在泡沫陶瓷表é¢çš"原ä¼zèŸè¼z½åŠå•è§å.	.0‰aå,⊐åŒ	E 2 空氒
204	Performance and mechanism of visible-light-induced plasmonic photocatalytic purification of NO with Ag/AgX. Chinese Science Bulletin, 2016, 61, 3482-3489.	0.7	2
205	Construction and Activity of an Allâ€Organic Heterojunction Photocatalyst Based on Melem and Pyromellitic Dianhydride. ChemSusChem, 2022, 15, .	6.8	2
206	Fabricating Z-scheme C-doped TiO ₂ /rGO nanocomposites for enhanced photocatalytic NO removal. Nanotechnology, 2022, 33, 415702.	2.6	2
207	Application Research at the Nano and Advanced Materials Institute. IEEE Nanotechnology Magazine, 2011, 5, 13-22.	1.3	1
208	Highly Efficient Photocatalytic Hydrogen Production Performance for 2D/0D g-C3N4/Zn0.5Cd0.5S with g-C3N4 as a Transport Medium for Photogenerated Charge Carriers. Journal of the Electrochemical Society, 0, , .	2.9	1
209	Unraveling the Reaction Mechanism of HCHO Catalytic Oxidation on Pristine Co3O4 (110) Surface: A Theoretical Study. Catalysts, 2022, 12, 560.	3.5	1

210 Welcome to the new journal Photocatalysis. , 0, , .

0